J. Fluid Mech. (1990), *vol.* 215, *pp.* 503–523
Printed in Great Britain

Nonlinear convection in a rigid channel uniformly heated from below

By P. G. DANIELS AND C. F. ONG
Department of Mathematics, City University, Northampton Square, London EC1V 0HB, UK

(Received 30 January 1989 and in revised form 24 November 1989)

A weakly nonlinear theory is developed for convection in an infinite rigid horizontal rectangular channel uniformly heated from below. A combination of analytical and numerical techniques along and in the cross-section of the channel leads to the derivation of an amplitude equation governing the spatial and temporal evolution of the flow above the critical Rayleigh number. Results are obtained for general Prandtl numbers and a wide range of aspect ratios. Overall trends are confirmed by comparison with results for an idealized model with stress-free horizontal boundaries. For wide channels, where the aspect ratio is large, the limiting form of the amplitude equation is predicted by reference to the two-dimensional equation describing roll patterns in infinite layers. The connection with this well-developed theory is established for both rigid and stress-free horizontal boundary conditions.

1. Introduction

This paper considers the onset of convection in an infinite rigid horizontal channel uniformly heated from below. The study is motivated by the desire to develop theoretical predictions of the motion near the onset of convection that can be compared with experimental results and are capable of describing initial transitions in the pattern of convective rolls. For low-Prandtl-number fluids contained in long boxes Buhler, Kirchartz & Oertel (1979) have observed a decrease in the number of rolls as the Rayleigh number is increased above its critical value, a behaviour confirmed qualitatively by Daniels & Chana (1987) using a simplified theoretical model with stress-free horizontal boundaries. The basis of this theoretical model is the amplitude equation that describes spatially modulated weakly nonlinear convection in an infinite channel. In the present work this equation is derived for the physically realistic case of rigid boundaries. It provides important information concerning the evolution, amplitude and waveband of stable convective states as a function of both the aspect ratio of the channel and the Prandtl number of the fluid.

The overall description of the flow is semi-analytical, a numerical approach being required to solve a succession of partial differential equations that arise in the cross-section of the channel. The first of these is the linear eigenvalue problem already considered by Luijkx & Platten (1981) for the case of insulating sidewalls and by Chana & Daniels (1989) for the case of conducting sidewalls. Galerkin methods were used in these studies and in the latter case results for the critical Rayleigh number and wavenumber were compared with asymptotic predictions at large and small aspect ratios. Comparisons of the critical wavelength with experiment have been made by Luijkx, Platten & Legros (1982). The main findings of the linear stability analysis and of experimental and numerical work, including that of Dubois & Berge

(1978) and Kessler (1987), confirm the original prediction of Davis (1967) that at the onset of motion the preferred mode of convection consists of rolls with axes aligned perpendicular to the sidewalls of the channel. These rolls are, however, a fully three-dimensional motion, with a non-zero velocity component perpendicular to the sidewalls.

The problem is formulated in §2. In §3 the extension of linearized theory to incorporate weakly nonlinear effects in the neighbourhood of the critical Rayleigh number is described. The coefficients of an amplitude equation for the spatial and temporal evolution of the nonlinear motion are determined in §4 using Galerkin representations of the various functions of the cross-channel coordinates. In §5, corresponding results for stress-free horizontal surfaces are presented. Here the partial differential equations can be reduced to ordinary ones and a 'finite-roll' representation allows approximate analytical expressions to be obtained for the coefficients of the amplitude equation. The results are particularly relevant at small and large aspect ratios where the cross-channel velocity component is small, and generally provide useful confirmation of the qualitative behaviour of the solution to the fully rigid problem.

For wide channels, limiting values of the coefficients of the amplitude equation are predicted from the known form of the equation governing two-dimensional roll patterns in infinite layers. The connection with this well-established theory for the infinite layer is not entirely straightforward and is described in §6 for the cases of both rigid and stress-free horizontal boundaries. The two cases are not identical. For stress-free boundaries the correct form of the amplitude equation for an infinite layer was found recently by Siggia & Zippelius (1981) and contains a term associated with the generation of vertical vorticity in the layer. This term was omitted in the earlier analysis of Newell & Whitehead (1969) and does not occur at the same level of approximation when the boundaries are rigid. Here it is shown that at finite aspect ratios the large-scale flow associated with this vertical vorticity is diminished in size and ceases to influence the main amplitude equation. A full discussion of the results is given in §7.

2. Formulation

Fluid is contained in an infinite horizontal rectangular channel $|y| \leqslant a$, $|z| \leqslant \frac{1}{2}$ where x, y, z are Cartesian coordinates non-dimensionalized with respect to the depth of the channel d, with the x-axis along the centre of the channel. In the Boussinesq approximation the governing equations may be written

$$\frac{\partial u}{\partial x}+\frac{\partial v}{\partial y}+\frac{\partial w}{\partial z}=0, \tag{2.1}$$

$$\nabla^2 u-\frac{\partial p}{\partial x}=N_1, \tag{2.2}$$

$$\nabla^2 v-\frac{\partial p}{\partial y}=N_2, \tag{2.3}$$

$$\nabla^2 w-\frac{\partial p}{\partial z}+R\theta=N_3, \tag{2.4}$$

$$\nabla^2 \theta+w=N_4, \tag{2.5}$$

where
$$(\sigma N_1, \sigma N_2, \sigma N_3, N_4) = \left\{\frac{\partial}{\partial t} + u\frac{\partial}{\partial x} + v\frac{\partial}{\partial y} + w\frac{\partial}{\partial z}\right\}(u, v, w, \theta). \tag{2.6}$$

Here θ and p are non-dimensional measures of the temperature θ^* and pressure p^* relative to the static, vertically stratified basic state:

$$\theta^* = \theta_0^* - \Delta\theta^* z + \Delta\theta^* \theta, \tag{2.7}$$

$$p^* = p_0^* - g\rho_0 z d(1 + \tfrac{1}{2}\alpha\Delta\theta^* z) + \rho_0 \kappa\nu d^{-2} p. \tag{2.8}$$

$\theta_0^* \mp \frac{1}{2}\Delta\theta^*$ are the constant temperatures of the upper and lower surfaces of the channel, ρ_0 is the fluid density at the mean temperature θ_0^*, g is the acceleration due to gravity, which acts in the negative z-direction, and α, ν and κ are the coefficient of thermal expansion, kinematic viscosity and thermal diffusivity of the fluid respectively. The velocity components u, v, w and time t are non-dimensionalized with respect to κ/d and d^2/κ and the Rayleigh number R and Prandtl number σ are defined by

$$R = \alpha g \Delta\theta^* d^3/\kappa\nu, \quad \sigma = \nu/\kappa. \tag{2.9}$$

For a channel with rigid perfectly conducting walls the boundary conditions at $y = \pm a (|z| \leqslant \frac{1}{2})$ and $z = \pm\frac{1}{2}(|y| \leqslant a)$ are

$$u = v = w = \theta = 0, \tag{2.10}$$

and since the primary interest is in applications to long totally enclosed boxes the volume flux down the channel must vanish,

$$\int_{-a}^{a}\int_{-\frac{1}{2}}^{\frac{1}{2}} u \, dy \, dz = 0. \tag{2.11}$$

Equations (2.1)–(2.5) and (2.10) can be recast in the form

$$\nabla^2\left(\frac{\partial^2 v}{\partial x^2} + \frac{\partial^2 v}{\partial y^2} + \frac{\partial^2 w}{\partial y \partial z}\right) = \frac{\partial^2 N_2}{\partial x^2} - \frac{\partial^2 N_1}{\partial x \partial y}, \tag{2.12}$$

$$\nabla^2\left(\frac{\partial^2 w}{\partial x^2} + \frac{\partial^2 w}{\partial z^2} + \frac{\partial^2 v}{\partial y \partial z}\right) + R\frac{\partial^2 \theta}{\partial x^2} = \frac{\partial^2 N_3}{\partial x^2} - \frac{\partial^2 N_1}{\partial x \partial z}, \tag{2.13}$$

$$\nabla^2\theta + w = N_4, \tag{2.14}$$

with
$$v = \frac{\partial v}{\partial y} = w = \theta = 0 \quad \text{on} \quad y = \pm a, \tag{2.15}$$

$$v = w = \frac{\partial w}{\partial z} = \theta = 0 \quad \text{on} \quad z = \pm\tfrac{1}{2}. \tag{2.16}$$

This provides a convenient framework within which to develop a weakly nonlinear theory amenable to a Galerkin representation of the functions v, w and θ.

3. Weakly nonlinear theory

Linear theory predicts that there is a critical Rayleigh number R_c, which depends only on the aspect ratio of the channel, at which the conductive state of no motion becomes unstable by an exchange process. For Rayleigh numbers

$$R = R_c + \epsilon, \tag{3.1}$$

where ϵ is small and positive, the fluid adopts a stationary three-dimensional roll pattern which can be found by expanding the solution in the form

$$(\theta, u, v, w, p) = \sum_{n=1} \epsilon^{n/2}(\theta_n, u_n, v_n, w_n, p_n)(x, y, z; X, \tau). \tag{3.2}$$

Here $X = \epsilon^{\frac{1}{2}}x$ and $\tau = \epsilon t$ are long length and time scales which allow for spatial modulation of the rolls about the critical wavelength and for a discussion of their evolution and stability.

At leading order

$$(\theta_1, u_1, v_1, w_1, p_1) = (\Theta, \mathrm{i}U, V, W, P)(y, z) A(X, \tau) \mathrm{e}^{\mathrm{i}q_c x} + \text{c.c.}, \tag{3.3}$$

where A is an unknown complex amplitude function, c.c. denotes complex conjugate and q_c is the critical wavenumber of the rolls. From (2.12)–(2.14) Θ, V and W are eigensolutions of the linearized system

$$\bar{\nabla}^2\left\{\left(\frac{\partial^2}{\partial y^2} - q^2\right)V + \frac{\partial^2 W}{\partial y\,\partial z}\right\} = 0, \tag{3.4}$$

$$\bar{\nabla}^2\left\{\left(\frac{\partial^2}{\partial z^2} - q^2\right)W + \frac{\partial^2 V}{\partial y\,\partial z}\right\} - Rq^2\Theta = 0, \tag{3.5}$$

$$\bar{\nabla}^2\Theta + W = 0, \tag{3.6}$$

$$V = \frac{\partial V}{\partial y} = W = \Theta = 0 \quad \text{on} \quad y = \pm a, \tag{3.7}$$

$$V = W = \frac{\partial W}{\partial z} = \Theta = 0 \quad \text{on} \quad z = \pm \tfrac{1}{2}, \tag{3.8}$$

where $\bar{\nabla}^2 = (\partial^2/\partial y^2) + (\partial^2/\partial z^2) - q^2$, evaluated at the minimum point of the neutral curve $R = R_c, q = q_c$. Solutions of this system for various aspect ratios have been obtained by Chana & Daniels (1989) and Daniels & Ong (1990); values of R_c and q_c are included in table 1 below. From (2.1) and (2.2)

$$U = \frac{1}{q}\left(\frac{\partial V}{\partial y} + \frac{\partial W}{\partial z}\right), \quad P = \frac{1}{q}\bar{\nabla}^2 U, \tag{3.9}$$

where $q = q_c$.

At order ϵ the leading contributions to the nonlinear functions

$$N_i = \sum_{j=1} \epsilon^{\frac{j+1}{2}} N_{ij},$$

together with derivatives in X, generate solutions of the form

$$\begin{aligned}(\theta_2, u_2, v_2, w_2, p_2) = \Big\{&(\Theta, \mathrm{i}U, V, W, P) B(X, \tau) \mathrm{e}^{\mathrm{i}q_c x} \\ &+ \mathrm{i}(\bar{\Theta}, \mathrm{i}\bar{U}, \bar{V}, \bar{W}, \bar{P}) \frac{\partial A}{\partial X} \mathrm{e}^{\mathrm{i}q_c x} + (\tilde{\Theta}, \mathrm{i}\tilde{U}, \tilde{V}, \tilde{W}, \tilde{P}) A^2 \mathrm{e}^{2\mathrm{i}q_c x} + \text{c.c.}\Big\} \\ &+ (\hat{\Theta}, \hat{U}, \hat{V}, \hat{W}, \hat{P}) |A|^2,\end{aligned} \tag{3.10}$$

where B is a further unknown complex amplitude function which does not influence the equation for A to be determined below and $\bar{\Theta}$, $\tilde{\Theta}$, $\hat{\Theta}$, $\bar{U}$ etc are real functions of

y and z. Only those functions associated with the nonlinear terms A^2 and $|A|^2$ depend on the Prandtl number, with the first set conveniently expressed as

$$(\tilde{\Theta}, \tilde{U}, \tilde{V}, \tilde{W}, \tilde{P}) = (\tilde{\Theta}_1, \tilde{U}_1, \tilde{V}_1, \tilde{W}_1, \tilde{P}_1) + \frac{1}{\sigma}(\tilde{\Theta}_2, \tilde{U}_2, \tilde{V}_2, \tilde{W}_2, \tilde{P}_2). \tag{3.11}$$

For the second set it is easily established from (2.2) and the flux constraint (2.11) (which implies that a pressure of order $\epsilon^{\frac{1}{2}}$ depending only on X and τ cannot occur) that $\hat{U} = 0$, and the cross-channel flow can be represented by a stream function $\hat{\Psi}$. From (2.3) and (2.4)

$$\frac{\partial \hat{P}}{\partial y} = \left(\frac{\partial^2}{\partial y^2} + \frac{\partial^2}{\partial z^2}\right)\hat{V} - \frac{2}{\sigma}\left(q_c UV + V\frac{\partial V}{\partial y} + W\frac{\partial V}{\partial z}\right), \tag{3.12}$$

$$\frac{\partial \hat{P}}{\partial z} = R_c\hat{\Theta} + \left(\frac{\partial^2}{\partial y^2} + \frac{\partial^2}{\partial z^2}\right)\hat{W} - \frac{2}{\sigma}\left(q_c UW + V\frac{\partial W}{\partial y} + W\frac{\partial W}{\partial z}\right), \tag{3.13}$$

and following the decomposition

$$(\hat{\Theta}, \hat{\Psi}) = (\hat{\Theta}_1, \hat{\Psi}_1) + \frac{1}{\sigma}(\hat{\Theta}_2, \hat{\Psi}_2) \tag{3.14}$$

and elimination of the pressure between (3.12) and (3.13) a pair of coupled systems, independent of the Prandtl number, is obtained for $\hat{\Theta}_i$ and $\hat{\Psi}_i$. The velocity field is then determined from $\hat{V}_i = \partial\hat{\Psi}_i/\partial z$, $\hat{W}_i = -\partial\hat{\Psi}_i/\partial y$ and the pressure (to within a function of integration depending on X and τ) from (3.12) and (3.13). Further details of the determination of the functions of y and z appearing in (3.10) are given in an Appendix.

At order $\epsilon^{\frac{3}{2}}$ solutions for v_3, w_3 and θ_3 contain components proportional to $e^{iq_c x}$ where the functions of y and z now satisfy the basic linear system (3.4)–(3.8) but with forcing terms $\chi_{1,2,3}$ on the right-hand sides of (3.4)–(3.6) respectively. These are generated by derivatives in X and τ as well as nonlinear contributions of order $\epsilon^{\frac{3}{2}}$ arising in N_i. The adjoint triplet associated with the basic linear system for V, W, Θ at the critical point is $(V, W, -q_c^2 R_c \Theta)$ so that the solvability condition is conveniently

$$\int_{-a}^{a}\int_{-\frac{1}{2}}^{\frac{1}{2}} (\chi_1 V + \chi_2 W - q_c^2 R_c \chi_3 \Theta)\, dy\, dz = 0. \tag{3.15}$$

This is automatically satisfied for the second-order system for $\bar{V}$, $\bar{W}$, $\bar{\Theta}$ but at this third stage the forms of $\chi_{1,2,3}$ imply that

$$\left(c_1 + \frac{c_2}{\sigma}\right)\frac{\partial A}{\partial \tau} = c_3 A + c_4\frac{\partial^2 A}{\partial X^2} - \left(c_5 + \frac{c_6}{\sigma} + \frac{c_7}{\sigma^2}\right)A|A|^2. \tag{3.16}$$

Formulae for the coefficients c_i, which depend only on the aspect ratio of the channel, are given in the Appendix.

4. Numerical procedure and results

The linear eigenfunctions may be represented by Galerkin series

$$\Theta = \sum_{k=1}^{N} a_k f_k(y,z), \quad W = \sum_{k=1}^{N} b_k g_k(y,z), \quad V = \sum_{k=1}^{N} c_k h_k(y,z) \tag{4.1}$$

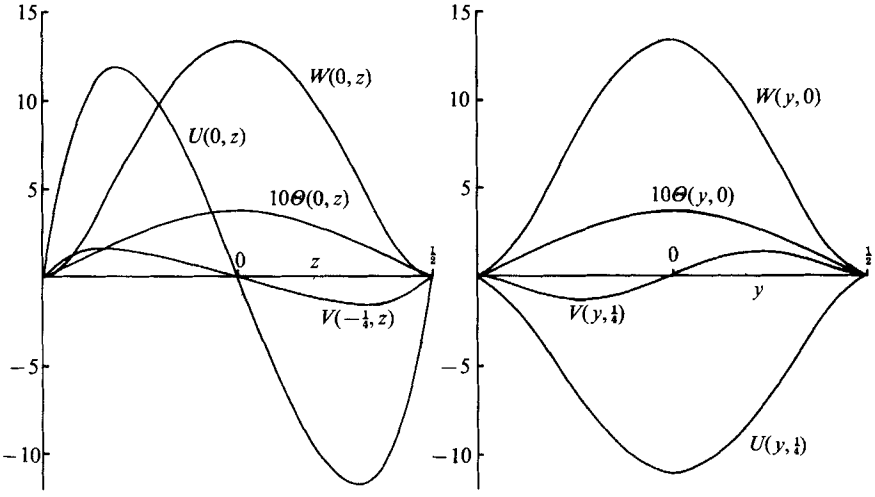

FIGURE 1. Leading-order temperature and velocity profiles for a square channel ($a = \frac{1}{2}$) based on the normalization $c_1 = 1$ with $N = 16$.

in which the trial functions are taken as

$$f_k = \cos(2m-1)\frac{\pi y}{2a}\cos(2n-1)\pi z, \tag{4.2}$$

$$g_k = \cos(2m-1)\frac{\pi y}{2a}C_n(z), \tag{4.3}$$

$$h_k = S_m\left(\frac{y}{2a}\right)\sin 2n\pi z. \tag{4.4}$$

Here C_n and S_m are the beam functions tabulated by Harris & Reid (1958) and the forms (4.2)–(4.4) are chosen to satisfy the boundary conditions (3.7), (3.8) and to have the symmetries in y and z associated with the leading eigenmode (Daniels & Ong 1990). The summations for $k = 1, \ldots, N$ are taken over all integer combinations m, n so that for $N = 16$, for example, all combinations of modes with $m, n \leqslant 4$ are included. Substitution of (4.1) into (3.4)–(3.6), multiplication by h_k, g_k and f_k ($k = 1, \ldots, N$) respectively and integration over the cross-section of the channel yields a set of $3N$ linear algebraic equations for the coefficients a_k, b_k, c_k which form the components of the column vector $\boldsymbol{x}$ in a matrix equation $\boldsymbol{C}\boldsymbol{x} = \boldsymbol{0}$. Zeros of the determinant of $\boldsymbol{C}$ are located to obtain the neutral curve $R(q)$ from which the critical values R_c and q_c are found. Even for $N = 10$ results appear to be accurate to within about $\frac{1}{4}\%$ and a truncation level $N = 16$ was generally used to obtain solutions to the succession of problems formulated in §3 and the Appendix. A normalization $c_1 = 1$ was adopted for the linearized solution V, W, Θ.

Solutions of the system (A 1)–(A 5) are sought in the form

$$\bar{\Theta} = \sum_{k=1}^{N} \bar{a}_k f_k(y,z), \quad \bar{W} = \sum_{k=1}^{N} \bar{b}_k g_k(y,z), \quad \bar{V} = \sum_{k=1}^{N} \bar{c}_k h_k(y,z) \tag{4.5}$$

and the Galerkin method applied with the same truncation level N to obtain the coefficients $\bar{a}_k, \bar{b}_k, \bar{c}_k$ from the matrix equation $\boldsymbol{C}\bar{\boldsymbol{x}} = \bar{\boldsymbol{B}}$, where $\bar{\boldsymbol{B}}$ contains the

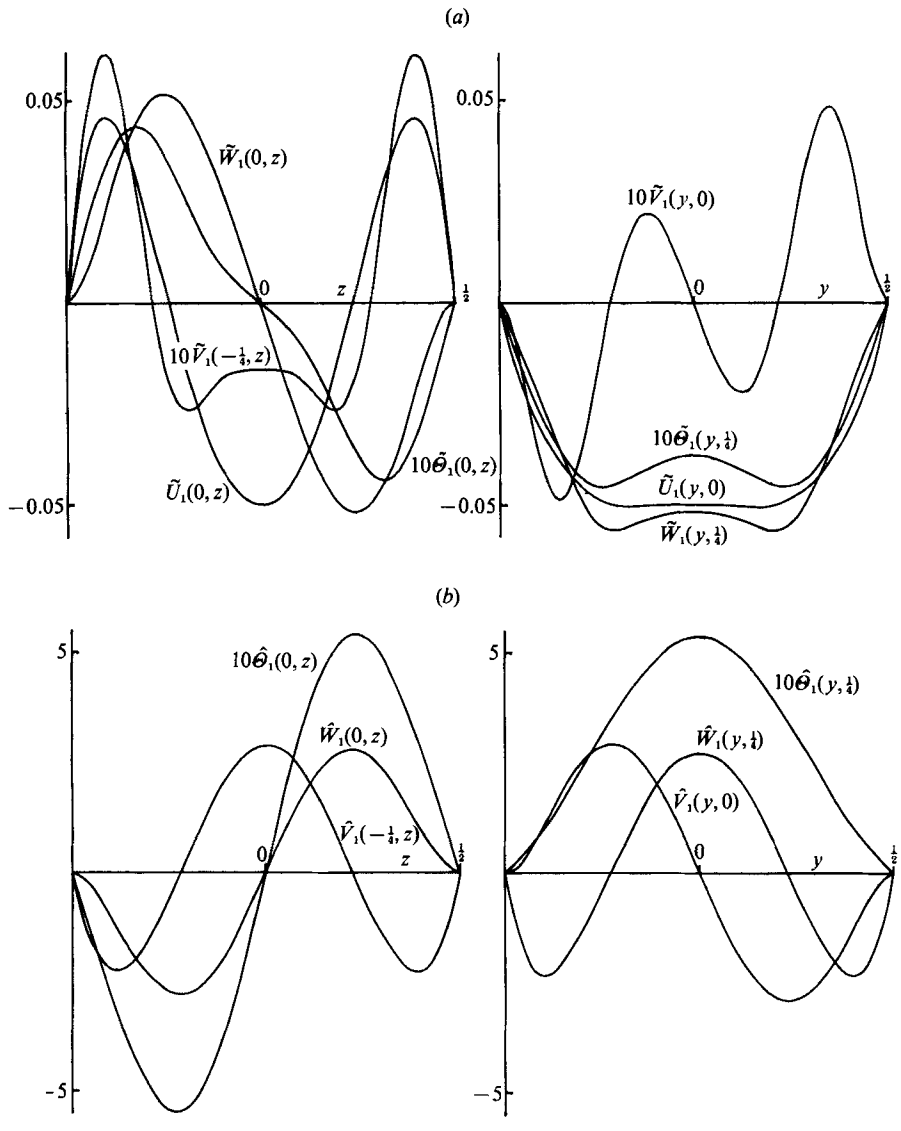

FIGURE 2. Prandtl-number-independent parts of the second-order temperature and velocity profiles associated with nonlinear effects for a square channel ($a = \frac{1}{2}$) based on the normalization $c_1 = 1$ with $N = 16$.

contributions from the right-hand sides of (A 1)–(A 3). The determinant of $\boldsymbol{C}$ is zero but a solution exists because the terms contributing to $\bar{\boldsymbol{B}}$ are consistent with the solvability condition (3.15). The solution was rendered unique by specifying $\bar{c}_1 = 0$ and Gaussian elimination used to triangularize $\boldsymbol{C}$, omitting the final (zero) row in the reduction process and confirming that (to within the expected tolerance) the corresponding term in the reduced form of $\bar{\boldsymbol{B}}$ was also zero. As a second check the first row of $\boldsymbol{C}$ was omitted from the reduction process and, on finding $\bar{a}_k, \bar{b}_k, \bar{c}_k$ from the remaining rows, checked against the value of $\bar{B}_1$.

The integrations involved in setting up the elements of $\boldsymbol{C}$ were performed using Simpson's rule, generally with 20 steps in both the y- and z-directions. Tests showed

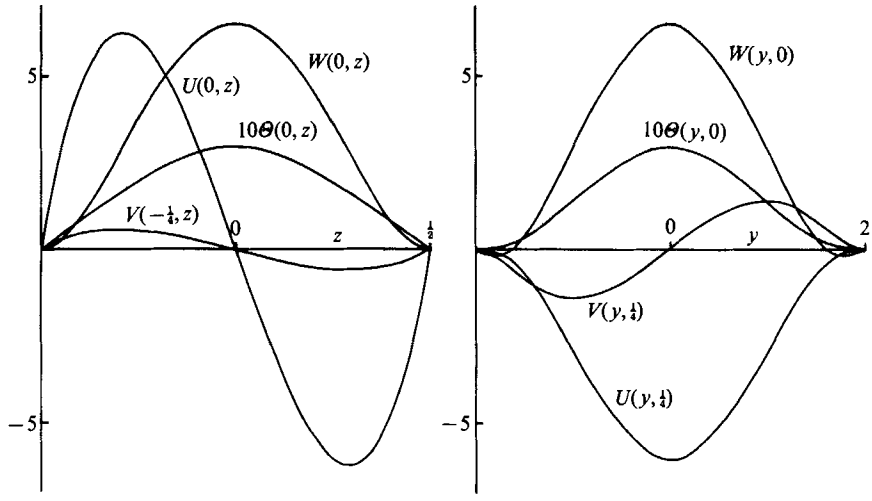

FIGURE 3. Leading-order temperature and velocity profiles for a relatively wide channel ($a = 2$) based on the normalization $c_1 = 1$ with $N = 16$.

that this generally produced elements accurate to about 5 significant figures. Although these elements can be converted into sums and products of one-dimensional integrals and thus evaluated most efficiently, it was decided to use direct two-dimensional integration in order to minimize the amount of algebraic manipulation involved. This is a significant simplification, particularly for calculations (below) involving as many as three products of the linear eigenfunctions. Subroutines were set up to evaluate these functions, their partial derivatives and subsequently determined functions at given values of y and z from stored values of the Galerkin coefficients. The same level of accuracy of integration was maintained throughout.

Solutions of the systems (A 9)–(A 13) are found in the form

$$\tilde{\Theta}_i = \sum_{k=1}^{N} \tilde{a}_{ki} \tilde{f}_k(y,z), \quad \tilde{W}_i = \sum_{k=1}^{N} \tilde{b}_{ki} \tilde{g}_k(y,z), \quad \tilde{V}_i = \sum_{k=1}^{N} \tilde{c}_{ki} \tilde{h}_k(y,z), \tag{4.6}$$

with the trial functions defined by

$$\tilde{f}_k = \cos(2m-1)\frac{\pi y}{2a} \sin 2n\pi z, \tag{4.7}$$

$$\tilde{g}_k = \cos(2m-1)\frac{\pi y}{2a} S_n(z), \tag{4.8}$$

$$\tilde{h}_k = S_m\left(\frac{y}{2a}\right) \cos(2n-1)\pi z, \tag{4.9}$$

taking into account boundary conditions and symmetry of the solution. Application of the Galerkin method leads to matrix equations $\boldsymbol{D}\tilde{\boldsymbol{x}} = \tilde{\boldsymbol{B}}_i$ which have unique solutions for the coefficients $\tilde{a}_{ki}$, $\tilde{b}_{ki}$, $\tilde{c}_{ki}$. Solutions of the systems (A 19)–(A 22) are found in the form

$$\hat{\Theta}_i = \sum_{k=1}^{N} \hat{a}_{ki} \hat{f}_k(y,z), \quad \hat{\Psi}_i = \sum_{k=1}^{N} \hat{d}_{ki} \hat{q}_k(y,z), \tag{4.10}$$

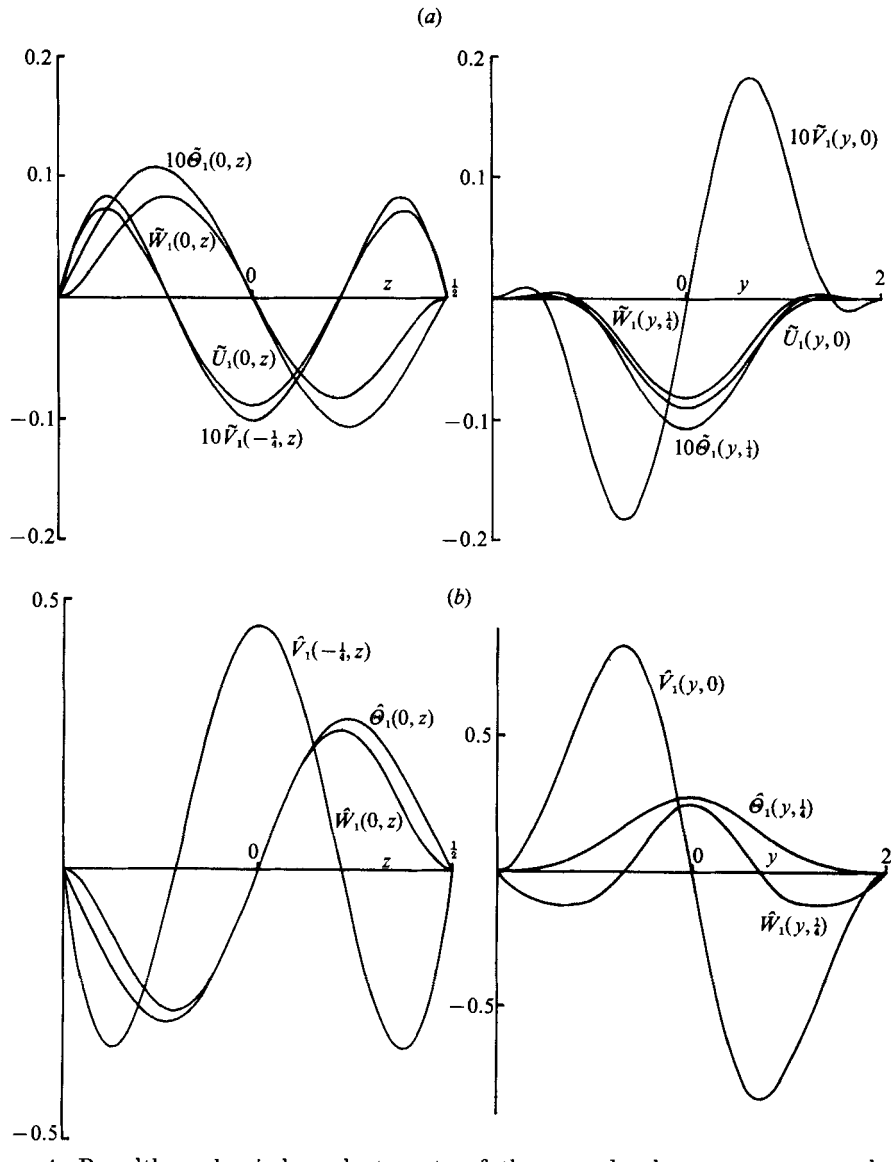

FIGURE 4. Prandtl-number-independent parts of the second-order temperature and velocity profiles associated with nonlinear effects for a relatively wide channel ($a = 2$) based on the normalization $c_1 = 1$ with $N = 16$.

with the trial functions defined by

$$\hat{f}_k = \cos(2m-1)\frac{\pi y}{2a}\sin 2n\pi z, \tag{4.11}$$

$$\hat{q}_k = S_m\left(\frac{y}{2a}\right)S_n(z). \tag{4.12}$$

Application of the Galerkin method leads to the straightforward calculation of the coefficients $\hat{a}_{ki}, \hat{d}_{ki}$ from a pair of matrix equations $\boldsymbol{E}\hat{\boldsymbol{x}} = \hat{\boldsymbol{B}}_i$. Finally the amplitude coefficients are evaluated numerically from (A 25)–(A 31) using Simpson's rule.

a	q_c	R_c	μ_1	μ_2	μ_3	$10^{-2}\mu_4$	$10^{-2}\mu_5$	$10^{-2}\mu_6$
0.125	5.524	56668	285.2	267.1	1743	9909	559.8	424.1
0.25	4.189	8959	133.3	107.8	644.4	1383	94.63	77.48
0.5	3.384	2946	93.68	59.35	328.3	337.2	25.45	23.97
1	2.951	1872	86.70	46.33	209.2	163.0	5.140	10.87
1.5	2.945	1744	86.73	44.88	200.1	149.2	2.941	7.426
2	2.997	1719	86.87	44.61	211.7	151.1	2.725	5.525
3	3.058	1710	86.88	44.49	227.8	155.8	1.548	3.683

TABLE 1. Critical parameters and amplitude coefficients for various aspect ratios a

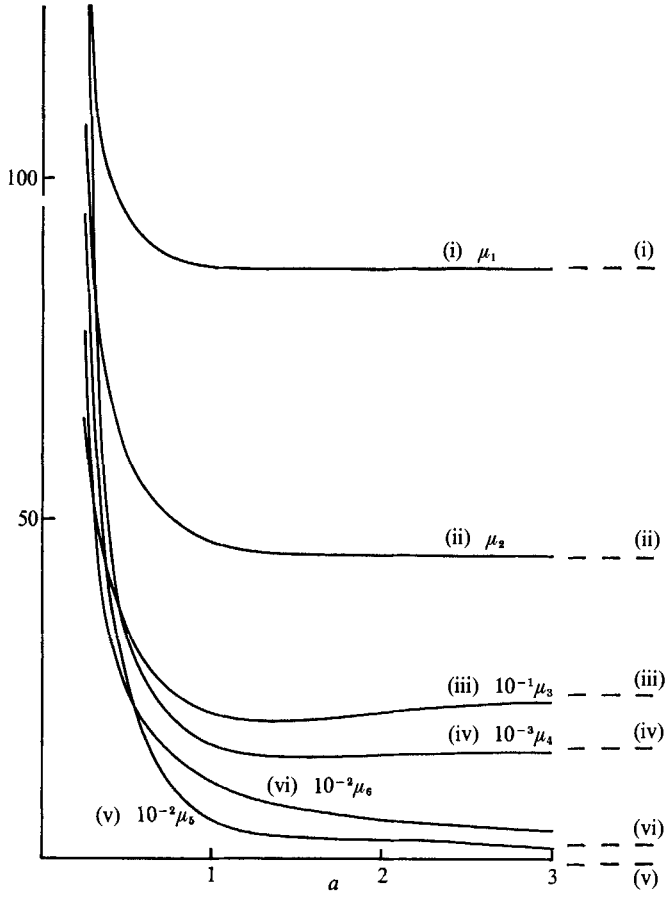

FIGURE 5. Coefficients of the amplitude equation (4.13) for a channel with rigid boundaries based on the normalization $\Theta(0,0) = 1$. The dashed lines are the asymptotes predicted in §6.

Figures 1–5 and table 1 contain a summary of the main results obtained for a truncation level $N = 16$ and various aspect ratios in the range $\frac{1}{8} \leqslant a \leqslant 3$. Various profiles in both the y- and z-directions for a square channel ($a = \frac{1}{2}$) and for a relatively wide channel, where $a = 2$, are shown in figures 1–4. Note the weak flow reversal near $y = \pm a$ in the latter case where a complicated three-dimensional sidewall motion, already identified as part of the linear solution by Chana & Daniels (1989), is evident.

The profiles displayed in figures 2 and 4 provide the amplitudes of the secondary velocity and temperature fields of non-critical wavelength generated in the channel for a fluid of infinite Prandtl number. One component consists of a three-dimensional motion of half the critical wavelength and the other is a two-dimensional motion independent of x consisting of four longitudinal rolls symmetrically placed in the four quadrants of the (y,z)-plane. Table 1 contains the major results of the analysis, giving both the critical parameter values and the amplitude coefficients for each aspect ratio. In order to facilitate a comparison with other results in §§5 and 6 it is convenient to adopt a new normalization $\Theta(0,0) = 1$ in (3.3), simply achieved by dividing the nonlinear coefficients $c_{5,6,7}$ by the actual value of $\{\Theta(0,0)\}^2$. In its simplest form the amplitude equation for A is then

$$\left(\mu_1+\frac{\mu_2}{\sigma}\right)\frac{\partial A}{\partial \tau} = A+\mu_3\frac{\partial^2 A}{\partial X^2}-\left(\mu_4+\frac{\mu_5}{\sigma}+\frac{\mu_6}{\sigma^2}\right)A|A|^2, \tag{4.13}$$

where the coefficients μ_i are shown in figure 5.

5. Stress-free horizontal surfaces

Further analytical progress is possible if the horizontal boundaries are taken to be stress-free planes in which case

$$w = \frac{\partial u}{\partial z} = \frac{\partial v}{\partial z} = \theta = 0 \quad \text{on} \quad z = \pm\tfrac{1}{2}. \tag{5.1}$$

The linear eigensolutions are now

$$(\Theta, W) = (\Theta_0, W_0)(y)\sin\pi\bar{z}, \quad (U, V) = (U_0, V_0)(y)\cos\pi\bar{z}, \tag{5.2}$$

where $\bar{z} = z+\frac{1}{2}$ and the critical Rayleigh number and wavenumber are those first obtained by Davies-Jones (1970) by solution of the ordinary differential eigenvalue problem

$$\left\{\left(\frac{\mathrm{d}^2}{\mathrm{d}y^2}-q^2-\pi^2\right)^3-R\left(\frac{\mathrm{d}^2}{\mathrm{d}y^2}-q^2\right)\right\}\Theta_0 = 0, \tag{5.3}$$

$$\left(\frac{\mathrm{d}^2}{\mathrm{d}y^2}-q^2-\pi^2\right)V_0 = \pi^{-1}\left\{\left(\frac{\mathrm{d}^2}{\mathrm{d}y^2}-q^2-\pi^2\right)^2-R\right\}\frac{\mathrm{d}\Theta_0}{\mathrm{d}y}, \tag{5.4}$$

$$\Theta_0 = \frac{\mathrm{d}^2\Theta_0}{\mathrm{d}y^2} = V_0 = \frac{\mathrm{d}V_0}{\mathrm{d}y} = 0 \quad (y = \pm a). \tag{5.5}$$

A normalization $\Theta_0(0) = 1$ is assumed, as in the derivation of (4.13). The amplitude equation equivalent to (4.13) has been obtained by Chana (1986), the various functions arising in the nonlinear analysis of §3 having simple dependencies on z: $\bar{\Theta}$, $\bar{W}$, $\bar{U}$ and $\bar{V}$ have forms similar to those in (5.2) above while $\tilde{\Theta}$, $\tilde{W}$, $\hat{\Theta}$ and $\hat{W}$ are proportional to $\sin 2\pi\bar{z}$. The function $\hat{V}$ is proportional to $\cos 2\pi\bar{z}$ as are $\tilde{U}$ and $\tilde{V}$ although these latter functions also contain additive components independent of $\bar{z}$. Figure 6 shows the coefficients of the amplitude equation for values of the aspect ratio in the range $\frac{1}{4} \leqslant a \leqslant 2$.

Even further progress can be made in the stress-free case by use of a technique

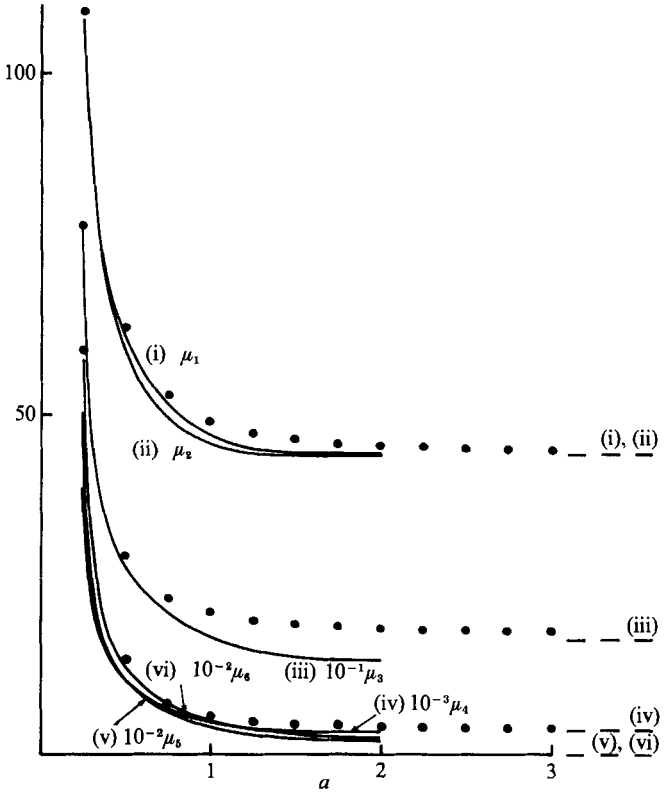

FIGURE 6. Coefficients of the amplitude equation (4.13) for a channel with stress-free horizontal boundaries based on the normalization $\Theta_0(0) = 1$. The dashed lines are the asymptotes predicted in §6 and the dots are the finite-roll approximations (5.9).

introduced by Davies-Jones (1970) known as the 'finite roll' approximation. This consists of setting the cross-channel velocity component v to zero and simply ignoring the y-component of the momentum equations. Then

$$\Theta_0 = \sin\frac{\pi}{2a}(y+a), \quad W_0 = \frac{\pi^2}{4}\left(\beta+3+\frac{1}{a^2}\right)\sin\frac{\pi}{2a}(y+a), \tag{5.6}$$

where $\beta = (9+2/a^2)^{\frac{1}{2}}$. Results of the linear theory described by Davies-Jones (1970) in which

$$R_c = \frac{\pi^4(\beta+3)}{16(\beta-1)}\left(\beta+3+\frac{1}{a^2}\right)^2, \quad q_c = \frac{\pi}{2}(\beta-1)^{\frac{1}{2}}, \tag{5.7}$$

are particularly accurate at both small and large aspect ratios (Chana 1986); for narrow channels the asymptotes $R_c \sim \pi^4/16a^4$, $q_c \sim \pi/2^{\frac{3}{4}}a^{\frac{1}{2}}$ given by (5.7) are numerically close to the actual asymptotes for free or rigid horizontal boundaries ($R_c \sim \pi^4/16a^4$, $q_c \sim (2\sqrt{3}/a)^{\frac{1}{2}}$ as $a \to 0$) while for wide channels the leading approximations to R_c and q_c coincide with those of the actual stress-free asymptotes

$$R_c \sim \tfrac{27}{4}\pi^4 + 193.36a^{-4}, \quad q_c \sim \frac{\pi}{\sqrt{2}} - 0.71933a^{-2}, \quad a \to \infty, \tag{5.8}$$

obtained by Chana & Daniels (1989). Extension of the finite-roll approximation to the nonlinear case leads to the following results for the coefficients of the amplitude equation (4.13):

$$\left.\begin{aligned} \mu_1 &= \mu_2 = \frac{\pi^2}{4}(\beta+3)\left(\beta+3+\frac{1}{a^2}\right)/(\beta-1), \\ \mu_3 &= \left(3\beta+9+\frac{2}{a^2}\right)\pi^2, \quad \mu_5 = \mu_6 = 0, \\ \mu_4 &= \frac{\pi^6(\beta+3)\left(\beta+3+\dfrac{1}{a^2}\right)^3}{256(\beta-1)(1+4a^2)^2}\left\{(1+4a^2)(1+6a^2)-\frac{\tanh 2\pi a}{2\pi a}\right\} \end{aligned}\right\} \tag{5.9}$$

(Chana 1986). It seems reasonable to expect qualitative agreement with both the rigid and stress-free results as $a \to 0$ and indeed the behaviours $\mu_1 = \mu_2 \sim \pi^2/4a^2$, $\mu_3 \sim 2\pi^2/a^2$, $\mu_4 \sim \pi^6(9+2\pi^2)/384a^4$ associated with (5.9) are consistent with the predictions of the Galerkin scheme at small aspect ratios. These results combined with those of the linear study by Chana & Daniels (1989) imply that in the rigid case $(\theta, u, v, w) = O((R-R_c)^{\frac{1}{2}}(a^2, a^{\frac{1}{2}}, a, 1))$ as $a \to 0$. At large aspect ratios the behaviours $\mu_1 = \mu_2 \sim 9\pi^2/2$, $\mu_3 \sim 18\pi^2$, $\mu_4 \sim 3^5\pi^6/4^3$ as $a \to \infty$ are in very good agreement with the exact stress-free calculations (see figure 6) although the numerical values of μ_3 and μ_4 would not be expected to tally precisely because the y-dependence assumed in (5.6) does not coincide with the actual y-variation of the linear solution at large aspect ratios (see below).

6. Asymptotic theory for wide channels $a \to \infty$

At large aspect ratios the present theory can be reconciled with the familiar two-dimensional amplitude equation describing roll patterns in an infinite horizontal layer, providing an important check on the results for both rigid and stress-free boundaries. For rigid horizontal boundaries this two-dimensional amplitude equation is

$$\left(\tilde{\mu}_1+\frac{\tilde{\mu}_2}{\sigma}\right)\frac{\partial \tilde{A}}{\partial \tilde{\tau}} = \tilde{\delta}\tilde{A}+\tilde{\mu}_3\left(\frac{\partial}{\partial \tilde{X}}-\frac{\mathrm{i}}{2q_0}\frac{\partial^2}{\partial \tilde{Y}^2}\right)^2\tilde{A}-\left(\tilde{\mu}_4+\frac{\tilde{\mu}_5}{\sigma}+\frac{\tilde{\mu}_6}{\sigma^2}\right)\tilde{A}|\tilde{A}|^2, \tag{6.1}$$

where

$$R = R_0 + a^{-4}\tilde{\delta}, \quad x = a^2\tilde{X}, \quad y = a\tilde{Y}, \quad t = a^4\tilde{\tau}, \tag{6.2}$$

$$\theta \sim a^{-2}\{\mathrm{e}^{\mathrm{i}q_0 x}\tilde{A}(\tilde{X}, \tilde{Y}, \tilde{\tau}) + \text{c.c.}\}\, g(z), \tag{6.3}$$

and $R_0 = 1707.76$ and $q_0 = 3.117$ are the critical Rayleigh number and wavenumber for the infinite layer. For convenience the solution here is expressed in terms of the large parameter a instead of the conventional small parameter $R-R_0$. A normalization $g(0) = 1$ is assumed and the coefficients

$$\tilde{\mu}_1 = 86.91, \quad \tilde{\mu}_2 = 44.47, \quad \tilde{\mu}_3 = 252.2, \quad \tilde{\mu}_4 = 22281, \quad \tilde{\mu}_5 = -150.37, \quad \tilde{\mu}_6 = 265.05, \tag{6.4}$$

may be inferred from previous work by Schluter, Lortz & Busse (1965), Kelly & Pal (1978), Wesfreid *et al.* (1978), Cross (1980) and Chana & Daniels (1989). The boundary conditions for (6.1) at the sidewalls of the channel are

$$\tilde{A} = \frac{\partial \tilde{A}}{\partial \tilde{Y}} = 0 \quad \text{at} \quad \tilde{Y} = \pm 1, \tag{6.5}$$

following the arguments of Brown & Stewartson (1977), as extended to the rigid case by Chana & Daniels (1989).

The coefficients (6.4) cannot be compared directly with the forms of those occurring in the one-dimensional amplitude equation (4.13) as $a \to \infty$ because in (4.13) the solution is expanded about the critical Rayleigh number $R_c(a)$ rather than R_0. This is equivalent in (6.2) and (6.3) to setting

$$\tilde{\delta} = \tilde{\mu}_3 q_0^{-2} \delta + \Delta, \tag{6.6}$$

with $\Delta = 0$ to correspond to $R = R_c(a)$ and

$$\tilde{A} = \Delta^{\frac{1}{2}} \tilde{A}_0 + \Delta \tilde{A}_1 + \Delta^{\frac{3}{2}} \tilde{A}_2 + \ldots, \quad \Delta \to 0. \tag{6.7}$$

At order $\Delta^{\frac{1}{2}}$, from (6.1),

$$\tilde{A}_0 = \bar{A}(\bar{X}, \bar{\tau}) F(\tilde{Y}) \, \mathrm{e}^{-\mathrm{i}\gamma \tilde{X}/q_0}, \tag{6.8}$$

where $\bar{X}$ and $\bar{\tau}$ are appropriate length and time scales defined by $\tilde{X} = \Delta^{-\frac{1}{2}} \bar{X}, \tilde{\tau} = \Delta^{-1} \bar{\tau}$ and

$$\left\{\left(\frac{1}{2}\frac{\mathrm{d}^2}{\mathrm{d}\tilde{Y}^2} + \gamma\right)^2 - \delta\right\} F = 0; \quad F = F' = 0 \quad (\tilde{Y} = \pm 1). \tag{6.9}$$

The required solution is

$$F = l \cos \omega_+ \tilde{Y} + (1 - l) \cosh \omega_- \tilde{Y}, \tag{6.10}$$

where

$$\omega_\pm = \sqrt{2}(\delta^{\frac{1}{2}} \pm \gamma)^{\frac{1}{2}} \quad \text{and} \quad l = (1 - \cos \omega_+ \operatorname{sech} \omega_-)^{-1} \tag{6.11}$$

to be consistent with the normalization $F = 1$ at $\tilde{Y} = 0$. The values of δ and γ needed in (6.6) and (6.8) are the solutions of the characteristic equation

$$\omega_- \tanh \omega_- + \omega_+ \tan \omega_+ = 0$$

for which δ is an absolute minimum. These are $\delta = \delta_c = 5.3708$ and $\gamma = \gamma_c = 1.5980$ (see Chana & Daniels 1989) and imply that

$$R_c \sim R_0 + \frac{\delta_c \tilde{\mu}_3}{q_0^2 a^4}, \quad q_c \sim q_0 - \frac{\gamma_c}{q_0 a^2}, \quad a \to \infty, \tag{6.12}$$

giving the corrections to the critical Rayleigh number and wavenumber due to the presence of the distant sidewalls.

At order Δ, (6.1) gives

$$\tilde{A}_1 = \left\{\bar{B}_0(\bar{X}, \bar{\tau}) F(\tilde{Y}) + \mathrm{i} \frac{\partial \bar{A}}{\partial \bar{X}} G(\tilde{Y})\right\} \mathrm{e}^{-\mathrm{i}\gamma \tilde{X}/q_0}, \tag{6.13}$$

where $\bar{B}_0$ is arbitrary at this stage and

$$\left\{\left(\frac{1}{2}\frac{\mathrm{d}^2}{\mathrm{d}\tilde{Y}^2} + \gamma\right)^2 - \delta\right\} G = -\left(\frac{\mathrm{d}^2}{\mathrm{d}\tilde{Y}^2} + 2\gamma\right) F; \quad G = G' = 0 \quad (\tilde{Y} = \pm 1). \tag{6.14}$$

The solution for G exists when $\delta = \delta_c$ and $\gamma = \gamma_c$ and can be expressed, without loss of generality, as $G = \partial F / \partial \gamma|_{\gamma_c}$, being given from (6.10) as

$$G = \beta_1(\cos \omega_+ \tilde{Y} - \cosh \omega_- \tilde{Y}) + \beta_2 \tilde{Y} \sin \omega_+ \tilde{Y} + \beta_3 \tilde{Y} \sinh \omega_- \tilde{Y}, \tag{6.15}$$

where $\beta_1 = \partial l / \partial \gamma$, $\beta_2 = -l/\omega_+$, $\beta_3 = (l-1)/\omega_-$ and all quantities are evaluated at $\gamma = \gamma_c$. At this point $\omega_+ = 2.7984$, $\omega_- = 1.1996$, $l = 0.65779$; $\beta_1 = -0.18516$, $\beta_2 = -0.23506$ and $\beta_3 = -0.28526$. Profiles of F and G are shown in figure 7.

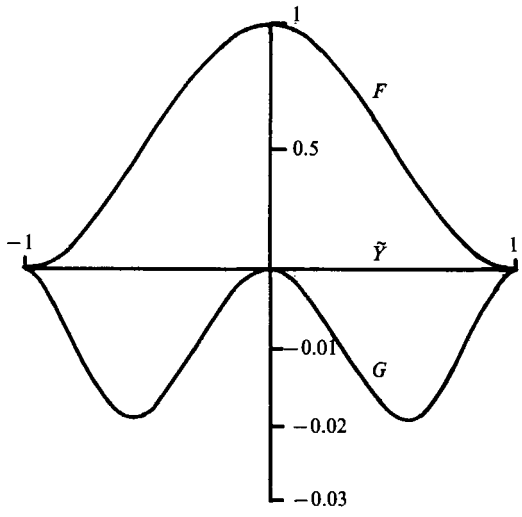

FIGURE 7. Profiles of the functions F and G at the critical point $\delta = \delta_c$, $\gamma = \gamma_c$.

At order $A^{\frac{3}{2}}$, (6.1) gives an equation for $\tilde{A}_2$ which has a solution satisfying $\tilde{A}_2 = \partial\tilde{A}_2/\partial\tilde{Y} = 0$ at $\tilde{Y} = \pm 1$ only if the solvability condition

$$\left(\tilde{\mu}_1 + \frac{\tilde{\mu}_2}{\sigma}\right)\frac{\partial \bar{A}}{\partial \bar{\tau}} = \bar{A} + \tilde{\mu}_3\left(1 + \frac{I_2}{I_1}\right)\frac{\partial^2 \bar{A}}{\partial \bar{X}^2} - \left(\tilde{\mu}_4 + \frac{\tilde{\mu}_5}{\sigma} + \frac{\tilde{\mu}_6}{\sigma^2}\right)\frac{I_3}{I_1}\bar{A}|\bar{A}|^2 \tag{6.16}$$

is satisfied, where

$$I_1 = \int_{-1}^{1} F^2 \,\mathrm{d}\tilde{Y}, \quad I_2 = \int_{-1}^{1} F\left(\frac{\mathrm{d}^2 G}{\mathrm{d}\tilde{Y}^2} + 2\gamma G\right)\mathrm{d}\tilde{Y}, \quad I_3 = \int_{-1}^{1} F^4 \,\mathrm{d}\tilde{Y} \tag{6.17}$$

and $\gamma = \gamma_c$. From (6.10) and (6.15) these integrals can be evaluated as $I_1 = 0.76741$, $I_2 = -0.03598$ and $I_3 = 0.56097$ and it is equation (6.16) that should be compared with the limiting form of (4.13) as $a \to \infty$, the parameter Δ/a^4 corresponding to ϵ in (3.1). The integral terms in (6.16) are the ones which prevent a simple comparison between the coefficients of the $\tilde{Y}$-independent terms in the two-dimensional amplitude equation (6.1) and those of (4.13) as $a \to \infty$. Thus the $\tilde{Y}$-dependence of the solution in the channel as $a \to \infty$ leads to modified values of the coefficients of both the spatial derivative and nonlinear terms in (6.1) given by

$$\tilde{\mu}_3\left(1 + \frac{I_2}{I_1}\right) = 240.4, \quad \left(\tilde{\mu}_4 + \frac{\tilde{\mu}_5}{\sigma} + \frac{\tilde{\mu}_6}{\sigma^2}\right)\frac{I_3}{I_1} = 16288 - \frac{109.92}{\sigma} + \frac{193.75}{\sigma^2}. \tag{6.18}$$

These values, together with those of μ_1 and μ_2, the coefficients of the time derivative which remain unmodified, are shown in figure 5 and compare well with the results of the Galerkin scheme for large a. Note that for a truly $\tilde{Y}$-independent solution of (6.1) where the sidewall boundary conditions are ignored, $F = 1$, $\gamma_c = \delta_c = 0$ and $G = 0$ giving $I_1 = I_3 = 2$ and $I_2 = 0$ in (6.17) and describing a bifurcation to two-dimensional rolls at $R = R_0$.

A similar analysis is possible for the case of stress-free horizontal boundaries and again satisfactory agreement is obtained. Here the two-dimensional amplitude

equation in the infinite layer is more complicated than that for the rigid problem (Siggia & Zippelius 1981) owing to the importance of a vertical vorticity $a^{-5}\Omega$ with Ω generated by a term

$$\tilde{A}^*\left(\frac{\partial}{\partial\tilde{X}}-\frac{\mathrm{i}}{2q_0}\frac{\partial^2}{\partial\tilde{Y}^2}\right)\tilde{A}+\text{c.c.}, \tag{6.19}$$

where * denotes complex conjugate. Here the notation is as in (6.1)–(6.3) but now $R_0 = 27\pi^4/4$ and $q_0 = \pi/\sqrt{2}$. The vorticity results in an additional contribution $i\tilde{B}\tilde{A}$ to the right-hand side of (6.1), $a^{-4}\tilde{B}(\tilde{X},\tilde{Y},\tilde{\tau})$ being the leading term of a non-oscillatory flow in the x-direction generated by Ω. However, substitution of the leading term of (6.7) into (6.19) shows that $\Omega = o(\Delta)$ in which case $\tilde{B} = o(\Delta)$ and $\tilde{B}\tilde{A} = o(\Delta^{\frac{3}{2}})$. The equation (6.16) is therefore unaffected by this additional contribution, a measure of the restriction imposed by the sidewalls of the channel. At finite aspect ratios the effect appears as a weak non-oscillatory flow u of order $\epsilon^{\frac{3}{2}}$ along the channel and thus influences both the amplitude equation for B in (3.10) and the wavelength selection process (Daniels & Chana 1987). For the stress-free case

$$\tilde{\mu}_1 = \tilde{\mu}_2 = \tfrac{9}{2}\pi^2, \quad \tilde{\mu}_3 = 18\pi^2, \quad \tilde{\mu}_4 = \tfrac{81}{16}\pi^6, \quad \tilde{\mu}_5 = \tilde{\mu}_6 = 0 \tag{6.20}$$

(Newell & Whitehead 1969) but otherwise the results (6.16), (6.17) still apply, with

$$\tilde{\mu}_3\left(1+\frac{I_2}{I_1}\right) = 169.32, \quad \left(\tilde{\mu}_4+\frac{\tilde{\mu}_5}{\sigma}+\frac{\tilde{\mu}_6}{\sigma^2}\right)\frac{I_3}{I_1} = 3557.8+\frac{0}{\sigma}+\frac{0}{\sigma^2}. \tag{6.21}$$

These values, together with those of μ_1 and μ_2 are shown in figure 6.

7. Discussion

Solutions have been obtained for the onset of three-dimensional convection in an infinite rigid channel with conducting sidewalls. The dependence of the solution on both the direction along the channel and the Prandtl number is determined analytically. The main results are contained within an amplitude equation whose coefficients have been calculated for all Prandtl numbers and a range of aspect ratios between $\frac{1}{4}$ and 6. Additional results for stress-free horizontal surfaces and asymptotic results for large aspect ratios have confirmed the general trend of the Galerkin calculations. The form of the amplitude equation is similar to that describing two-dimensional roll patterns in an infinite layer (Newell & Whitehead 1969; Daniels 1977) so that general properties of the solution are modified only by changes of scale. In particular, the coefficients μ_1 and μ_2 provide a measure of the timescale $t \sim (R-R_c)^{-1}(\mu_1+\sigma^{-1}\mu_2)$ on which small disturbances develop near the critical Rayleigh number, while μ_3 determines the waveband of nonlinear stationary states $|q-q_c| < (R-R_c)^{\frac{1}{2}}\mu_3^{-\frac{1}{2}}$ as $R \to R_c$. Those solutions for which $|q-q_c| < (R-R_c)^{\frac{1}{2}}(3\mu_3)^{-\frac{1}{2}}$ are stable to the sideband instability discussed by Eckhaus (1965). Other oblique modes of instability discussed by Newell & Whitehead (1969) within the context of the two-dimensional amplitude equation are not relevant near R_c when a is finite. The maximum amplitude of the motion corresponds to the solution

$$|A| = \left(\mu_4+\frac{\mu_5}{\sigma}+\frac{\mu_6}{\sigma^2}\right)^{-\frac{1}{2}} \equiv \hat{a}$$

when $q = q_c$ and the perturbation temperature field and vertical velocity attain maximum values

$$\theta_{\max} \sim 2\hat{a}(R-R_c)^{\frac{1}{2}}, \quad w_{\max} \sim 2\hat{a}\left\{\frac{W(0,0)}{\Theta(0,0)}\right\}(R-R_c)^{\frac{1}{2}} \tag{7.1}$$

on the centre of the channel.

Unfortunately results of full numerical simulations by Oertel (1980), largely consistent with experiments by Dubois & Berge (1978), are only available for comparison at relatively large aspect ratios. For air ($\sigma = 0.71$) Oertel found that $\theta_{\max} \approx 0.12$ at $R \approx 1815$ and that $w_{\max} \approx 9$ and 18 at $R \approx 3000$ and 5000 respectively. Using the fact that for $a = 2$, $W(0,0)/\Theta(0,0) \approx 22$ (see figure 3), the leading approximations (7.1) give corresponding values of 0.15, 12 and 20. In fact it is not surprising that infinite-layer theory based on (6.1) is more accurate for such a large aspect ratio, giving corresponding results

$$\theta_{\max} \sim 2(R-R_0)^{\frac{1}{2}}\left(\tilde{\mu}_4+\frac{\tilde{\mu}_5}{\sigma}+\frac{\tilde{\mu}_6}{\sigma^2}\right)^{-\frac{1}{2}} \approx 0.14 \quad \text{and} \quad w_{\max} \approx 10 \quad \text{and} \quad 16.$$

The reason for this is that the expansion (3.2) is only valid at large aspect ratios a when $R-R_c \ll a^{-4}$. Thus as a increases, the range of validity of the one-dimensional amplitude equation (4.13) is restricted to a diminishing neighbourhood of the critical Rayleigh number R_c. On the extended range $R-R_c = O(a^{-4})$ the full amplitude equation (6.1) comes into operation and the linear profile $F(\tilde{Y})$ is replaced by a uniform profile as $(R-R_0)a^4 \to \infty$. Boundary layers of thickness $y \pm a = O((R-R_0)^{-\frac{1}{4}})$ then provide adjustment to the sidewall boundary conditions (6.5). The failure of (4.13) is equivalent to the requirement that $A \ll 1$ in (6.6) but, formally, the breakdown of the basic expansion (3.2) follows from the fact that $\Theta = O(1)$ and $\bar{\Theta} = O(a^2)$ as $a \to \infty$, so that the expansion fails when $\epsilon^{\frac{1}{2}} \sim a^{-2}$. This can be seen from (A 6) in combination with (6.12), or by estimating the effect of the inhomogeneous terms in (A 1)–(A 3) as $a \to \infty$. Note that in (A 28) the coefficient c_4 remains $O(a)$ as $a \to \infty$ because the leading contributions of $O(a^3)$ coincide with the leading terms on the left-hand side of the solvability condition (3.15).

The present results may be adapted to the case of a long box $|x| < L$, say, with $L \gg 1$, in a straightforward manner. Previous theories (Daniels 1977, 1978) have developed an understanding of how endwalls at $x = \pm L$ affect the onset of two-dimensional rolls parallel to those walls, the $\tilde{Y}$-independent form of (6.1) providing a basis for the theory. The main effect of the presence of the endwalls is simply that the amplitude function must vanish at $x = \pm L$, and this identifies the onset of motion to within an accuracy of $O(L^{-2})$ in the Rayleigh number. It is expected that the same remains true in the case of the channel except that the appropriate amplitude equation is now (4.13). The relevant solution is the leading mode of the steady linearized version of (4.13) for which $A = 0$ at $X = \pm\epsilon^{\frac{1}{2}}L$ so that the onset of stationary convection occurs in a long box when

$$R \sim R_c + \frac{\pi^2}{4}\mu_3 L^{-2}, \quad L \gg 1, \tag{7.2}$$

with both R_c and μ_3 dependent on the aspect ratio a.

The theory for two-dimensional rolls with stress-free horizontal surfaces has actually been extended to include an important class of nonlinear solutions which

arises when $R-R_0 = O(L^{-1})$ (Cross *et al.* 1983; Daniels 1981). The corresponding waveband $|q-q_0| = O(L^{-1})$ allows solution states with different numbers of rolls and transitions between these states can be identified as the value of the Rayleigh number changes (Daniels 1984). Motions in long rigid boxes exhibit such transitions at low Prandtl numbers (Buhler *et al.* 1979) and it is hoped that eventually the present theory can be extended to provide a quantitative comparison. Daniels & Chana (1987) have indicated how this might be done but the main requirements, which are the coefficients of the higher-order amplitude equation for B in (3.10) and certain constants associated with the solution near the endwalls at $x = \pm L$, present a formidable task. In principle, however, the Galerkin method described here could be used to carry out the necessary calculations. Experimental results for relatively small values of a and very large values of L would be most amenable to comparison. The present method has the advantage that the structure of the entire family of stationary states can be determined near the critical Rayleigh number (Daniels & Chana 1987) in contrast to the computationally expensive requirement of tracing even a single solution branch by a fully numerical three-dimensional treatment. It is expected that a similar technique to that used here would be useful for other weakly nonlinear stability problems provided the system is sufficiently extended in one direction.

This work was supported by a research grant from the Science and Engineering Research Council.

Appendix

The system for $\bar{\Theta}$, $\bar{V}$ and $\bar{W}$ obtained from (2.12)–(2.16) is

$$\bar{\nabla}^2\left\{\left(\frac{\partial^2}{\partial y^2}-q_c^2\right)\bar{V}+\frac{\partial^2\bar{W}}{\partial y\,\partial z}\right\} = -2q_c\left\{\left(\frac{\partial^2}{\partial y^2}-q_c^2\right)V+\frac{\partial^2 W}{\partial y\,\partial z}+\bar{\nabla}^2 V\right\}, \tag{A 1}$$

$$\bar{\nabla}^2\left\{\left(\frac{\partial^2}{\partial z^2}-q_c^2\right)\bar{W}+\frac{\partial^2\bar{V}}{\partial y\,\partial z}\right\}-R_c q_c^2\bar{\Theta} = -2q_c\left\{R_c\Theta+\left(\frac{\partial^2}{\partial z^2}-q_c^2\right)W+\frac{\partial^2 V}{\partial y\,\partial z}+\bar{\nabla}^2 W\right\}, \tag{A 2}$$

$$\bar{\nabla}^2\bar{\Theta}+\bar{W} = -2q_c\Theta, \tag{A 3}$$

$$\bar{V} = \frac{\partial\bar{V}}{\partial y} = \bar{W} = \bar{\Theta} = 0 \quad (y = \pm a), \tag{A 4}$$

$$\bar{V} = \bar{W} = \frac{\partial\bar{W}}{\partial z} = \bar{\Theta} = 0 \quad (z = \pm\tfrac{1}{2}), \tag{A 5}$$

and it is seen from (3.4)–(3.8) that a solution is

$$\bar{\Theta} = -\left.\frac{\partial\Theta}{\partial q}\right|_{q_c}, \quad \bar{V} = -\left.\frac{\partial V}{\partial q}\right|_{q_c}, \quad \bar{W} = -\left.\frac{\partial W}{\partial q}\right|_{q_c}, \tag{A 6}$$

where Θ, V, W are here regarded as the solutions of (3.4)–(3.8) at general points on the neutral stability curve $R = R(q)$, the condition $\mathrm{d}R/\mathrm{d}q = 0$ being satisfied at the critical point. Also

$$\bar{U} = \frac{1}{q_c}\left(\frac{\partial\bar{V}}{\partial y}+\frac{\partial\bar{W}}{\partial z}+U\right) = -\left.\frac{\partial U}{\partial q}\right|_{q_c} \tag{A 7}$$

and
$$\bar{P} = \frac{1}{q_c}(\bar{\nabla}^2\bar{U} + P + 2q_c U) = -\left.\frac{\partial P}{\partial q}\right|_{q_c}. \tag{A 8}$$

The solutions (A 6)–(A 8) may contain in addition an arbitrary multiple of the corresponding basic linear eigensolution although this may be considered part of the solution associated with B.

From (2.12)–(2.16), for $i = 1, 2$

$$\tilde{\nabla}^2\left\{\left(\frac{\partial^2}{\partial y^2} - 4q_c^2\right)\tilde{V}_i + \frac{\partial^2 \tilde{W}_i}{\partial y\,\partial z}\right\} = \tilde{\chi}_{i1}, \tag{A 9}$$

$$\tilde{\nabla}^2\left\{\left(\frac{\partial^2}{\partial z^2} - 4q_c^2\right)\tilde{W}_i + \frac{\partial^2 \tilde{V}_i}{\partial y\,\partial z}\right\} - 4q_c^2 R_c\,\tilde{\Theta}_i = \tilde{\chi}_{i2}, \tag{A 10}$$

$$\tilde{\nabla}^2\tilde{\Theta}_i + \tilde{W}_i = \tilde{\chi}_{i3}, \tag{A 11}$$

where $\tilde{\nabla}^2 = \partial^2/\partial y^2 + \partial^2/\partial z^2 - 4q_c^2$,

$$\tilde{V}_i = \frac{\partial \tilde{V}_i}{\partial y} = \tilde{W}_i = \tilde{\Theta}_i = 0 \quad (y = \pm a), \tag{A 12}$$

$$\tilde{V}_i = \tilde{W}_i = \frac{\partial \tilde{W}_i}{\partial z} = \tilde{\Theta}_i = 0 \quad (z = \pm \tfrac{1}{2}), \tag{A 13}$$

$\tilde{\chi}_{11} = \tilde{\chi}_{12} = \tilde{\chi}_{23} = 0$, and

$$\tilde{\chi}_{13} = -q_c U\Theta + V\frac{\partial \Theta}{\partial y} + W\frac{\partial \Theta}{\partial z}, \tag{A 14}$$

$$\tilde{\chi}_{21} = 4q_c^2\left(q_c UV - V\frac{\partial V}{\partial y} - W\frac{\partial V}{\partial z}\right) + 2q_c\frac{\partial}{\partial y}\left(V\frac{\partial U}{\partial y} + W\frac{\partial U}{\partial z} - q_c U^2\right), \tag{A 15}$$

$$\tilde{\chi}_{22} = 4q_c^2\left(q_c UW - V\frac{\partial W}{\partial y} - W\frac{\partial W}{\partial z}\right) + 2q_c\frac{\partial}{\partial z}\left(V\frac{\partial U}{\partial y} + W\frac{\partial U}{\partial z} - q_c U^2\right). \tag{A 16}$$

Also, from (2.1)

$$\tilde{U}_i = \frac{1}{2q_c}\left(\frac{\partial \tilde{V}_i}{\partial y} + \frac{\partial \tilde{W}_i}{\partial z}\right) \quad (i = 1, 2) \tag{A 17}$$

and from (2.2)

$$\tilde{P}_1 = \frac{1}{2q_c}\tilde{\nabla}^2\tilde{U}_1, \quad \tilde{P}_2 = \frac{1}{2q_c}\left(\tilde{\nabla}^2\tilde{U}_2 + q_c U^2 - V\frac{\partial U}{\partial y} - W\frac{\partial U}{\partial z}\right). \tag{A 18}$$

From (3.12), (3.13) and (2.5), for $i = 1, 2$

$$\hat{\nabla}^4\hat{\Psi}_i - R_c\frac{\partial \hat{\Theta}_i}{\partial y} = \hat{\chi}_{i1}, \tag{A 19}$$

$$\hat{\nabla}^2\hat{\Theta}_i - \frac{\partial \hat{\Psi}_i}{\partial y} = \hat{\chi}_{i2}, \tag{A 20}$$

where $\hat{\nabla}^2 = \partial^2/\partial y^2 + \partial^2/\partial z^2$,

$$\hat{\Theta}_i = \hat{\Psi}_i = \frac{\partial \hat{\Psi}_i}{\partial y} = 0 \quad (y = \pm a), \tag{A 21}$$

$$\hat{\Theta}_i = \hat{\Psi}_i = \frac{\partial \hat{\Psi}_i}{\partial z} = 0 \quad (z = \pm \tfrac{1}{2}), \tag{A 22}$$

$\hat{\chi}_{11} = \hat{\chi}_{22} = 0$, and

$$\hat{\chi}_{12} = 2\left(q_c U\Theta + V\frac{\partial\Theta}{\partial y} + W\frac{\partial\Theta}{\partial z}\right), \tag{A 23}$$

$$\hat{\chi}_{21} = 2\frac{\partial}{\partial z}\left(q_c UV + V\frac{\partial V}{\partial y} + W\frac{\partial V}{\partial z}\right) - 2\frac{\partial}{\partial y}\left(q_c UW + V\frac{\partial W}{\partial y} + W\frac{\partial W}{\partial z}\right). \tag{A 24}$$

The amplitude coefficients arising in (3.16) are

$$c_1 = \int_{-a}^{a}\int_{-\frac{1}{2}}^{\frac{1}{2}} q_c^2 R_c \Theta^2 \,\mathrm{d}y\,\mathrm{d}z, \tag{A 25}$$

$$c_2 = \int_{-a}^{a}\int_{-\frac{1}{2}}^{\frac{1}{2}} \left(q_c^2 V^2 + q_c^2 W^2 - q_c V\frac{\partial U}{\partial y} - q_c W\frac{\partial U}{\partial z}\right)\mathrm{d}y\,\mathrm{d}z, \tag{A 26}$$

$$c_3 = \int_{-a}^{a}\int_{-\frac{1}{2}}^{\frac{1}{2}} q_c^2 \Theta W \,\mathrm{d}y\,\mathrm{d}z, \tag{A 27}$$

$$c_4 = \int_{-a}^{a}\int_{-\frac{1}{2}}^{\frac{1}{2}} \{L_1 V + L_2 W + q_c^2 R_c(\Theta - 2q_c\bar{\Theta})\Theta\}\,\mathrm{d}y\,\mathrm{d}z, \tag{A 28}$$

$$c_5 = \int_{-a}^{a}\int_{-\frac{1}{2}}^{\frac{1}{2}} q_c^2 R_c L_{41}\Theta \,\mathrm{d}y\,\mathrm{d}z, \tag{A 29}$$

$$c_6 = \int_{-a}^{a}\int_{-\frac{1}{2}}^{\frac{1}{2}} \left\{\left(q_c^2 L_{21} - q_c\frac{\partial L_{11}}{\partial y}\right)V + \left(q_c^2 L_{31} - q_c\frac{\partial L_{11}}{\partial z}\right)W + q_c^2 R_c L_{42}\Theta\right\}\mathrm{d}y\,\mathrm{d}z, \tag{A 30}$$

$$c_7 = \int_{-a}^{a}\int_{-\frac{1}{2}}^{\frac{1}{2}} \left\{\left(q_c^2 L_{22} - q_c\frac{\partial L_{12}}{\partial y}\right)V + \left(q_c^2 L_{32} - q_c\frac{\partial L_{12}}{\partial z}\right)W\right\}\mathrm{d}y\,\mathrm{d}z, \tag{A 31}$$

where

$$\left.\begin{aligned} L_1 &= 2q_c\left\{\left(2\frac{\partial^2}{\partial y^2} + \frac{\partial^2}{\partial z^2} - 2q_c^2\right)\bar{V} + \frac{\partial^2\bar{W}}{\partial y\,\partial z}\right\} - \left(2\frac{\partial^2}{\partial y^2} + \frac{\partial^2}{\partial z^2} - 6q_c^2\right)V - \frac{\partial^2 W}{\partial y\,\partial z}, \\ L_2 &= 2q_c\left\{\left(\frac{\partial^2}{\partial y^2} + 2\frac{\partial^2}{\partial z^2} - 2q_c^2\right)\bar{W} + \frac{\partial^2\bar{V}}{\partial y\,\partial z} + R_c\bar{\Theta}\right\} - \left(\frac{\partial^2}{\partial y^2} + 2\frac{\partial^2}{\partial z^2} - 6q_c^2\right)W - \frac{\partial^2 V}{\partial y\,\partial z} - R_c\Theta, \end{aligned}\right\} \tag{A 32}$$

and $\bar{N}_{i2} = \sigma^{-1}L_{i1} + \sigma^{-2}L_{i2}$ $(i = 1, 2, 3), \bar{N}_{42} = L_{41} + \sigma^{-1}L_{42}$ where L_{ij} are independent of σ and

$$\sigma\bar{N}_{12} = q_c U\tilde{U} + V\frac{\partial\tilde{U}}{\partial y} - \tilde{V}\frac{\partial U}{\partial y} + \hat{V}\frac{\partial U}{\partial y} + W\frac{\partial\tilde{U}}{\partial z} - \tilde{W}\frac{\partial U}{\partial z} + \hat{W}\frac{\partial U}{\partial z}, \tag{A 33}$$

$$\left.\begin{aligned} &(\sigma\bar{N}_{22}, \sigma\bar{N}_{32}, \bar{N}_{42}) = (\mathscr{L}(V), \mathscr{L}(W), \mathscr{L}(\Theta)); \\ &\mathscr{L}(\zeta) = 2q_c U\tilde{\xi} + q_c\tilde{U}\zeta + V\frac{\partial\tilde{\xi}}{\partial y} + \tilde{V}\frac{\partial\zeta}{\partial y} + W\frac{\partial\tilde{\xi}}{\partial z} + \tilde{W}\frac{\partial\zeta}{\partial z} + V\frac{\partial\hat{\xi}}{\partial y} + \hat{V}\frac{\partial\zeta}{\partial y} + W\frac{\partial\hat{\xi}}{\partial z} + \hat{W}\frac{\partial\zeta}{\partial z}. \end{aligned}\right\} \tag{A 34}$$

REFERENCES

BROWN, S. N. & STEWARTSON, K. 1977 *Stud. Appl. Maths* **57**, 187.

BUHLER, K., KIRCHARTZ, K. R. & OERTEL, H. 1979 *Acta Mech.* **31**, 155.

CHANA, M. S. 1986 Thermal convection in channels and long boxes. Ph.D. thesis, City University, London.

CHANA, M. S. & DANIELS, P. G. 1989 *J. Fluid Mech.* **199**, 257.

CROSS, M. C. 1980 *Phys. Fluids* **23**, 1727.

CROSS, M. C., DANIELS, P. G., HOHENBERG, P. C. & SIGGIA, E. D. 1983 *J. Fluid Mech.* **127**, 155.

DANIELS, P. G. 1977 *Proc. R. Soc. Lond.* A **358**, 173.

DANIELS, P. G. 1978 *Mathematika* **25**, 216.

DANIELS, P. G. 1981 *Proc. R. Soc. Lond.* A **378**, 539.

DANIELS, P. G. 1984 *J. Fluid Mech.* **143**, 125.

DANIELS, P. G. & CHANA, M. S. 1987 *Proc. ASME Winter Annual Meeting, Boston. HTD*, vol. 94, p. 49.

DANIELS, P. G. & ONG, C. F. 1990 *Intl J. Heat Mass Transfer* **33**, 55.

DAVIES-JONES, R. P. 1970 *J. Fluid Mech.* **44**, 695.

DAVIS, S. H. 1967 *J. Fluid Mech.* **30**, 465.

DUBOIS, M. & BERGE, P. 1978 *J. Fluid Mech.* **85**, 641.

ECKHAUS, W. 1965 *Studies in Nonlinear Stability Theory*. Springer.

HARRIS, D. L. & REID, W. H. 1958 *Astrophys. J. Suppl. Ser.* **3**, 429.

KELLY, R. E. & PAL, D. 1978 *J. Fluid Mech.* **86**, 433.

KESSLER, R. 1987 *J. Fluid Mech.* **174**, 357.

LUIJKX, J. M. & PLATTEN, J. K. 1981 *J. Non-Equilib. Thermodyn.* **6**, 141.

LUIJKX, J. M., PLATTEN, J. K. & LEGROS, J. C. 1982 *Intl J. Heat Mass Transfer* **25**, 1252.

NEWELL, A. C. & WHITEHEAD, J. A. 1969 *J. Fluid Mech.* **38**, 279.

OERTEL, H. 1980 In *Natural Convection in Enclosures* (ed. K. E. Torrance & I. Catton), vol. 8, p. 11. ASME HTD.

SCHLUTER, A., LORTZ, D. & BUSSE, F. H. 1965 *J. Fluid Mech.* **23**, 129.

SIGGIA, E. D. & ZIPPELIUS, A. 1981 *Phys. Rev. Lett.* **47**, 835.

WESFREID, J., POMEAU, Y., DUBOIS, M., NORMAND, C. & BERGE, P. 1978 *J. Phys. Lett.* **39**, 725.